PRECISE RANGE ESTIMATION ON KNOWN SURFACES BY ANALYSIS OF FULL-WAVEFORM LASER

B. Jutzi [a], U. Stilla [b]

[a] FGAN-FOM Research Institute for Optronics and Pattern Recognition, 76275 Ettlingen, Germany - jutzi@fom.fgan.de
[b] Photogrammetry and Remote Sensing, Technische Universitaet Muenchen, 80290 Muenchen, Germany - stilla@bv.tum.de

Commission III, WG III/3

KEY WORDS: Accuracy, Analysis, Laser scanning, LIDAR, Measurement, Full-waveform.

ABSTRACT:

Laser range data analysis is of high interest in photogrammetry. Range estimation for complex surface structures can be inaccurate. To overcome this drawback a method using a laser scanner capable of full-waveform analysis is proposed. For analysis the transmitted waveform of the emitted pulse is used to estimate the received waveform of the backscattered pulse for a known surface. We simulated a plane surface with different slopes and a sphere. Typical spatial beam distributions are considered for modeling, namely Gaussian and uniform. The surface response is determined and the corresponding received waveform is calculated. The normalized cross-correlation function in between the simulated and the measured waveform is used for precise range measurement. Additionally the position on the surface can be determined.

1. INTRODUCTION

The automatic generation of 3-d models for a description of man-made objects, like buildings, is of great interest in photogrammetric research. Laser scanner systems allow a direct and illumination-independent measurement of the range. Laser scanners capture the range of 3-d objects in a fast, contact free and accurate way. Overviews for laser scanning systems are given in (Huising & Pereira, 1998; Wehr & Lohr, 1999; Baltsavias, 1999). A general overview on how to develop and design laser systems can be found in textbooks (Jelalian, 1992; Kamermann, 1993).

Current pulsed laser scanner systems for topographic mapping are based on time-of-flight techniques to determine the range of the illuminated object. The elapsed time between the emitted and backscattered laser pulses is typically determined by a threshold detection with analog electronics. Some systems capture multiple reflections caused by objects which are smaller than the laser beam footprint located in different ranges. Such systems usually record the first and the last backscattered laser pulse.

First pulse as well as last pulse exploitation is used for different applications like urban planning or forestry surveying. While first pulse registration is the optimum choice to measure the hull of partially penetrable objects (e.g. canopy of trees), last pulse registration should be chosen to measure non-penetrable surfaces (e.g. ground surface below vegetation).

Beside the first or last pulse exploitation the complete waveform in between is of interest, because it includes the backscattering characteristic of the illuminated field. Investigations on the waveform analysis were done to explore the vegetation concerning the bio mass, foliage or density (e.g. trees, bushes, and ground). NASA has developed a prototype of the Laser Vegetation Imaging Sensor (LVIS) recording the waveform to determine the vertical density profiles in forests (Blair *et al.*, 1999). This experimental airborne system operates at altitudes up to 10 km and provides a large footprint diameter (up to 80 m) to study different land cover classes.

The spaceborne Geoscience Laser Altimeter System (GLAS) on Ice, Cloud and land Elevation Satellite (ICESat) determines changes in range through time, height profiles of clouds and aerosols, ice sheet and land elevations, and vegetation (Brenner *et al.*, 2003; Zwally *et al.*, 2002). It operates with a large footprint diameter (70 m) on Earth and measures elevation changes with decimeter accuracy (Hoften *et al.*, 2000).

Beside large footprint systems first developments of small footprint systems were done for monitoring the nearshore bathymetric environments with the Scanning Hydrographic Operational Airborne Lidar Survey system (SHOALS). SHOALS has been in full operation since 1994 (Irish & Lillycrop, 1999; Irish *et al.*, 2000). Recent developments of commercial airborne laser scanner systems led to systems that allow capturing the waveform: LITEMAPPER 5600, OPTECH ALTM 3100, TOPEYE II, and TOPOSYS HARRIER 56. The systems mentioned above are specified to operate with a transmitted pulse width of 4-10 ns and allow digitization and acquisition of the waveform with approximately 0.5-1 GSample/s.

To interpret the received waveform of the backscattered pulse, a fundamental understanding of the physical background of pulse propagation and surface interaction is important (Jutzi *et al.*, 2002; Wagner *et al.*, 2003). The influence of the surface on the transmitted waveform is discussed by Steinvall (2000) for objects with different shapes taking into account different reflection characteristics. Gardner (1982) and Bufton (1989) investigated the pulse spreading by the impact of the surface structure, e.g. surface slope and vertical roughness within the laser footprint.

The recording of the received waveform offers the possibility to use different methods for the range determination, e.g. peak detection, leading edge detection, average time value detection, constant fraction detection. This topic was investigated by different authors, e.g. Der *et al.*, 1997; Steinvall & Carlsson, 2001; Jutzi & Stilla, 2003; Thiel & Wehr, 2004; Wagner *et al.*, 2004; Vandapel *et al.*, 2004. The analysis of the pulse shape increases the reliability, accuracy, and resolution.

The range estimation is further improved by the comparison between the transmitted and the received waveform. This can be done by signal processing methods (e.g. cross-correlation, inverse filtering), if the sampling of the waveform is done with

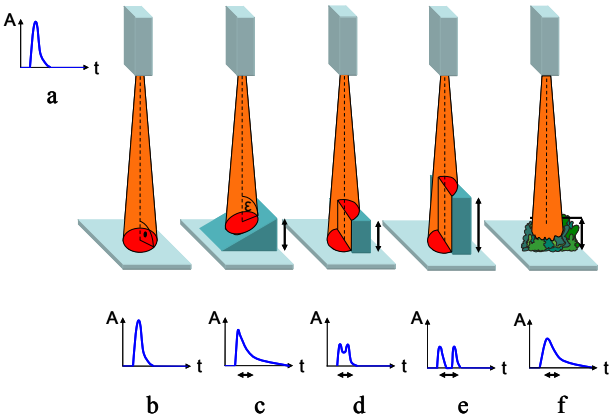

Figure 1. Effects of the surface on the received waveform.
a) transmitted waveform,
b) plane surface,
c) sloped surface,
d) two slightly different elevated areas,
e) two significantly different elevated areas,
f) randomly distributed small objects.

a high sampling rate. The maximum of the cross-correlation between the transmitted and received signal estimates the range value with a higher reliability and accuracy than considering the received waveform only (Hofton & Blair, 2001; Jutzi & Stilla, 2005; Thiel *et al.*, 2005).

Beside the range determination further surface features can be studied by waveform analysis, namely *reflectance*, *slope* and *roughness*. This specific surface features have an influence on the *amplitude* and *width* of the received waveform (Brenner *et al.*, 2003; Jutzi & Stilla 2002; Steinvall et al., 2004; Wagner *et al.*, 2006). For a parametric description of the pulse properties a Gaussian decomposition method on the waveform can be used (Hofton *et al.*, 2000; Jutzi & Stilla 2005; Persson *et al.*, 2005; Söderman *et al.*, 2005). Nowadays, waveform analysis is more and more established for remote sensing applications especially in forestry (Hug *et al.*, 2004; Reitberger *et al.*, 2006).

Depending on the application different surfaces have to be analyzed, e.g. for urban objects we have to deal with different elevated objects. In rural environment we have to deal with statistically distributed natural objects. The impact of the scene on the received waveform will be discussed using some standard examples (Figure 1). Different elevated object surfaces within the beam corridor lead to a mixture of different range values. A simple situation is given by a horizontal plane surface which will lead to a small pulse (Figure 1b). A plane which is slanted in relation to the viewing direction shows different range values within the footprint. This range interval which is given by the size of the footprint and the orientation of the plane leads to a spread of the pulse width (Figure 1c). A deformation of the pulse form can also be caused by perpendicularly oriented plane surfaces shifted by a small step in viewing direction (Figure 1d). A large step leads to two separate pulses (Figure 1e). Several surfaces with different range within the beam can result in multiple pulses. Randomly distributed small objects (e.g. by vegetation) spread over different range values within the beam leads as well to a spread of the pulse width (Figure 1f). These examples show the influence on the waveform by standard surface situations. The energy distribution within the beam was not considered. For predicting received waveforms of more complex surfaces and different energy distributions a modeling and simulation of the process is required.

The modeling of the received waveform can be done when the surface is known. A typical situation where known surfaces can be used is for registration of multiple scans received from different positions or at a different time. In these cases typically retro-reflective markers in form of spheres, cylinders or planes are used (Dold, 2005) and a precise range estimation of the known surfaces are helpful for the registration process. Beside this the surface has not to be known in advance, it can be estimated by previous measurements. Then a possible refinement of each range value can be done under consideration of the surface geometry in the close neighborhood.

In Section 2, an overview on the simulation setup is given. We simulated the surface response for different slopes and a spherical surface, which is shown in Section 3. For known surface structures corresponding received waveforms can be calculated and compared with measured waveforms, which is presented in Section 4. By proofing these waveforms for similarity the position on the surface and the precise range value can be determined.

2. SIMULATION

The simulation is necessary to estimate the received waveform of the backscattered pulse received from a known surface. For the transmitted waveform of the emitted pulse a measured or a modeled waveform can be used.

By the use of a 3-d *object representation* for the object model (Figure 2-1) and the *extrinsic orientation* parameter for sensor position and orientation (Figure 2-2), the model is *sampled* to get a high-resolution range and reflectance image (Figure 2-3). The resolution has to be higher than the scanning grid we want to simulate for further processing. Considering the transmitted waveform of the emitted pulse and the spatial energy distribution of the laser beam for temporal and spatial *laser pulse properties* is relevant for modeling the laser pulse (Figure 2-4). To simulate the *scanning* of the laser system, the values of grid spacing and the divergence of the laser beam are used for convolving the high-resolution range image with the transmitted waveform and convolving the high-resolution reflectance image with the spatial energy distribution of the beam (Figure 2-5). For a range depending *1-d surface representation*, the surface response is determined by the spatial undersampling of the high resolution range and intensity image (Figure 2-6). By convolving the surface response with the transmitted waveform the received waveform is determined at the *receiver* (Figure 2-7).

For simulating the received waveform of the backscattered pulses an *object model* (Section 2.1) and a *sensor model* (Section 2.2) is required.

2.1 Object modeling

For a 3-d object representation, our simulation setup considers geometric and radiometric features of the illuminated surface in the form of 3-d object models with homogeneous surface reflectance.

The object model with homogeneous surface reflectance is then sampled higher than the scanning grid we simulate and process, because with the higher spatial resolution we simulate the spatial distribution of the laser beam. Considering the position and orientation of the sensor system we receive a high-resolution range image and reflectance image. Depending on

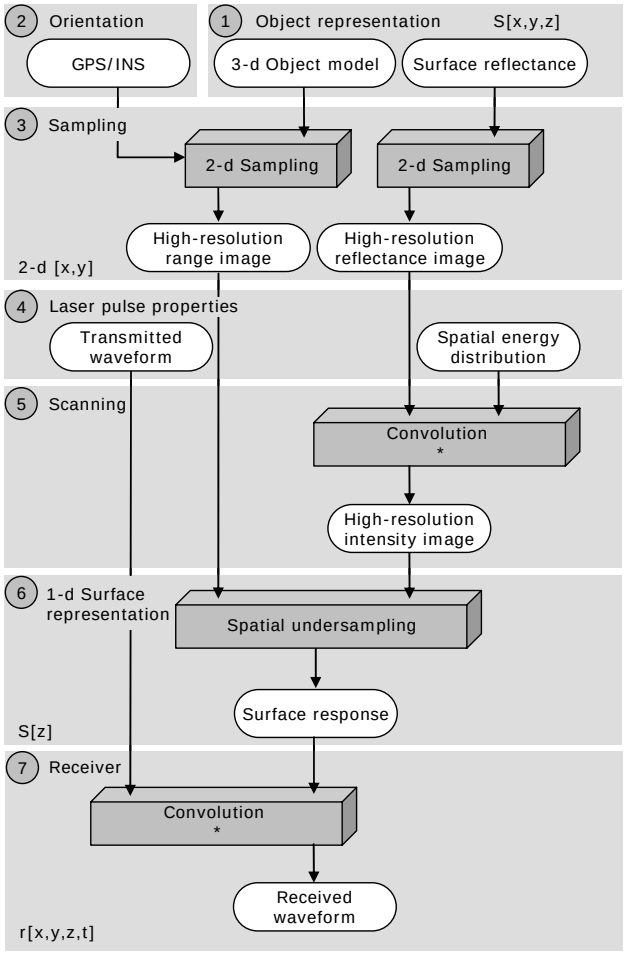

Figure 2. Simulation setup for calculating the received waveform.

the predetermined position and orientation of the sensor system, various range images can be captured.

2.2 Sensor modeling

The sensor model takes into account the specific properties of the sensing process: the position and orientation of the sensor, the laser pulse description, the scanning process and the electrical receiver properties. To simulate various aspects, a description of the extrinsic orientation of the laser scanning system with a GPS/INS system is used.

The emitted laser pulse of the system is characterized by specific pulse properties (Jutzi *et al.*, 2003). We assume radial symmetric uniform spatial distributions and radial symmetric Gaussian distributions for the beam profile, which are typical for the most laser systems. For this simulation we use measured transmitted waveforms to have a realistic description, where the bandwidth of the receiver to capture the waveform is 6 GHz and the data is sampled with 20 GSample/s. The transmitted waveform of the used system shows strong intensity fluctuations from pulse to pulse (Figure 3). The high sampling rate provides detailed information about the shape of the waveform with at least 100 sampling points for the typical length of the pulse (5 ns at Full-width-at-half-maximum).

Depending on the scan pattern of the laser scanner system, the grid spacing of the scanning process, and the divergence of the laser beam, a sub-area of the high-resolution range and reflectance images is processed. Therefore, the sub-area of the high-resolution reflectance image is convolved with the spatial energy distribution of the laser beam (distribution at the grid line $\pm 2\sigma$) to take into account the amount of backscattered laser light for each reflectance value. By focusing the beam with its specific properties on the detector of the receiver, the spatial resolution is reduced and this is simulated with a spatial undersampling of the sub-areas. Therefore the received high-resolution intensity and range image is processed by spatial undersampling to gain a weighted 1-d range distribution, which we call surface response. The determined surface response is convolved with the transmitted waveform to gain the received waveform of the backscattered pulse.

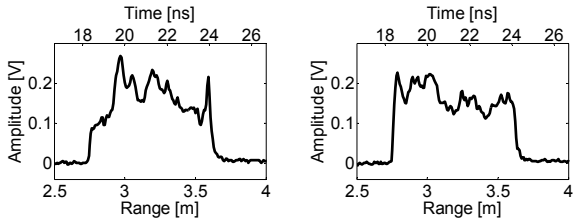

Figure 3. Two samples of the transmitted waveform.

3. CALCULATING THE SURFACE RESPONSE

The received waveform of a laser pulse depends on the transmitted waveform $s[t]$, the impulse response $h[t]$ of the receiver unit, the spatial beam distribution of the used laser $P[x,y]$, and the illuminated surface $S[x,y,z]$. The received waveform $r[x,y,z,t]$ can be expressed by a convolution of the relevant terms mentioned above and we get

$$r[x,y,z,t] = s[t] * h[t] * P[x,y] * S[x,y,z] , \quad (1)$$

where (*) denotes the convolution operation. The impulse response is mainly effected by the used photodiode and amplifier, the spatial beam distribution has typically the shape of a Gaussian or uniform, and the surface characteristic can be described by its geometry and reflectance properties (mixture of diffuse and specular). We assume to have a receiver unit consisting out of an ideal photodiode and amplifier with an infinite bandwidth and a linear frequency characteristic. The 3-d surface characteristic can be reduced to a range depending 1-d signal $S[z]$, which we call in this paper surface response.

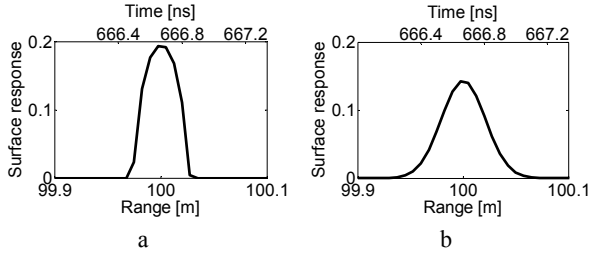

Figure 4. Examples of two surface responses for a slope with 25 degrees and different spatial beam distributions:
a) uniform,
b) Gaussian.

To study the surface response received from different surfaces, we simulated a plane surface which can be adjusted for various slopes illuminated by a beam with a spatial *uniform beam distribution* and a *Gaussian beam distribution*. Further surface responses from a small sphere with a radius of 0.3 m are determined by illuminating the surface of the sphere at different

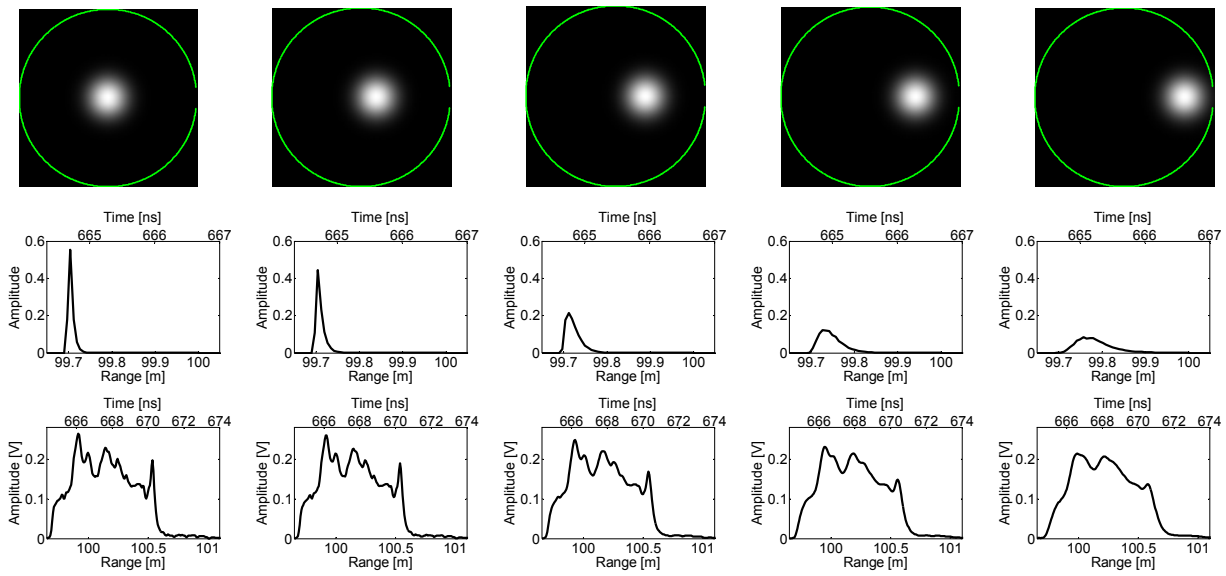

Figure 5. Position of the beam on the sphere (top row), corresponding surface responses (middle row); and the estimated received waveform (bottom row).
a) $p_0 = 0$ (center), b) $p_1 = 1/6\ r$, c) $p_2 = 2/6\ r$, d) $p_3 = 3/6\ r$, e) $p_4 = 4/6\ r$.

positions. For the simulation, the laser beam divergence is set to 1 mrad and the spatial range spacing for processing the surface response is 7.5 mm, which is equivalent to 20 GSample/s.

3.1 Plane surface with slope

We simulated a system illuminating a plane surface with different slopes. Therefore a high-resolution range image with 300x300 pixels of the sloped surfaces is calculated to determine the surface response. For surface reflectance a homogenous surface with 100% reflectance was assumed. The distance to the surface center is 100 m.

Examples of the calculated surface response $S[z]$ in dependence of the range z for a slope of 25 degrees received from an uniform beam distribution and a Gaussian beam distribution is shown in Figures 4a and 4b. The maximum of the surface response is at the range of 100m.

3.2 Spherical surface

A high-resolution range image with 300x300 pixels of a small sphere with its origin at the coordinate (0, 0, 100 m) and a radius r = 0.3 m is generated. Assuming a *Gaussian beam distribution* the surface response is calculated for five sampling positions [p_0, p_1, p_2, p_3, p_4] distributed equidistantly from the center p_0 to the boundary of the sphere. For the spacing of the sampling we chose 0.5 mrad, which is approximately equivalent to 1/6 of the radius r.

The Figure 5 shows at the top row the position of the beam on the sphere, where the boundary of the sphere is visualized by a bright line. The diagrams in the middle show the corresponding surface response. With the calculated surface response the estimated received waveform for the different positions is calculated by convolving the surface response with the transmitted waveform. For exemplary waveform we selected the transmitted waveform which is depicted in Figure 3a. The received waveforms are shown in Figure 5 at the lower row. If the footprint is located at the sphere center (Figure 5a, top row) the received waveform (Figure 5a, lower row) is very similar to the transmitted waveform (Figure 3a). By shifting the footprint away from the sphere center the received waveform (Figure 5b-e, lower row) is getting more and more smeared.

4. ESTIMATING THE POSITION AND RANGE

First the transmitted and the received waveform has to be measured (Figure 6-1) with the receiver unit of the laser system. Then by the use of the transmitted waveform and the determined surface response (Figure 6-2) for each position on the surface the estimated received waveform (Figure 6-3) can be calculated by a convolution. These estimated received waveforms calculated for different positions on the surface are compared with the measured waveform by determining different normalized cross-correlation functions. With the maximum coefficient of the normalized cross-correlation functions the most likely position and the accurate range of the surface can be determined (Figure 6-4). Figure 6 depicts a schematic description of the processing chain.

4.1 Matched filter

The data analysis starts with the detection of the backscattered pulses in the temporal signal. Usually this signal is disturbed by various noise components: background radiation, amplifier

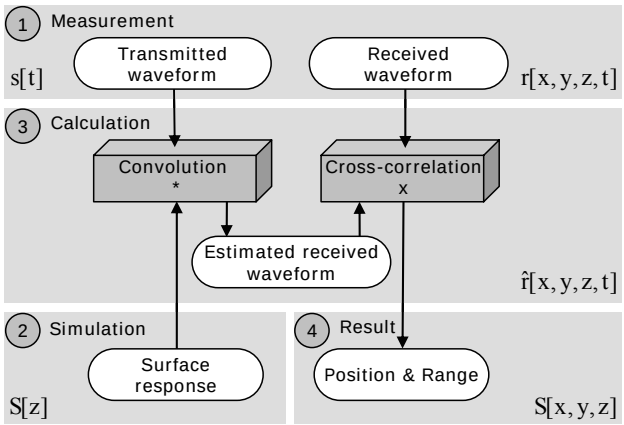

Figure 6. Processing chain to estimate position and range.

noise, photo detector noise etc. Detecting the received waveform of the backscattered pulse in noisy data and extracting the associated travel time is a well-known problem and is discussed in detail in radar techniques (Skolnik, 1980) and system theory (Papoulis, 1984). Due to this problem matched filters are used.

To improve the range accuracy and the signal-to-noise ratio (*SNR*) the matched filter for the waveform of the backscattered pulse has to be determined. In practice, it is difficult to determine the optimal matched filter. In cases where no optimal matched filter is available, sub-optimum filters may be used, but at the cost of decreasing the SNR. If the temporal deformation of the received signal can be neglected and the waveform is uniformly attenuated (isotropic attenuation by reflection or transmission of the pulse) the transmitted waveform of the emitted pulse is the best choice for the matched filter coefficients determination. In practice, the temporal deformation by the surface is common phenomenon (Figure 1). In this paper, we focus on determining this optimal filter by calculating the estimated received waveform, which can be expected from a known surface.

Let us assume that the noise components of the system mentioned above are sufficiently described by white noise with the constant factor *N*. Furthermore the signal energy of the pulse is defined as *E*. The maximum *SNR* occurs if the signal and the filter match. In this case the associated travel time *t* of the delayed pulse is τ and the *SNR* is described by

$$SNR\,[\tau] = \frac{2E}{N} \tag{2}$$

An interesting fact of this result is that the maximum of the instantaneous *SNR* depends only on the signal energy of the emitted pulse and the noise, and is independent of the shape.

Generally the matched filter is computed by the normalized cross-correlation function R_{sr} between the transmitted waveform $s[t]$ of the emitted pulse and the estimated received waveform $\hat{r}[x, y, z, t]$ of the backscattered pulse. Assuming zero-mean waveforms, we obtain the output signal $k[t]$ with a local maximum at the delay time τ

$$k[\tau] = R_{sr}[t+\tau] = \frac{\sum_{t=0}^{M-1} s[t] \cdot \hat{r}[x, y, z, t+\tau]}{\sqrt{\sum_{t=0}^{M-1} s[t]^2 \cdot \sum_{t=0}^{M-1} \hat{r}[x, y, z, t]^2}}, \tag{3}$$

where *M* is the length of the correlation function $k[\tau]$.

Then the output signal $k[t]$ with improved SNR is analyzed by a detection filter searching for the local maximum to determine the travel time of the pulse. By using the correlation signal to calculate the travel time, a higher accuracy is reached than by operating on the waveform, because exploiting the shape of the pulse waveform instead of a single value increases the accuracy (Jutzi & Stilla, 2005). This is because the specific pulse properties (e.g. asymmetric shape, intensity fluctuations) are taken into account and so less temporal jitter for range estimation can be expected.

4.2 Processing the position and range

The waveform received from an unknown position on the surface is given by the measurement. To determine the position on the surface, the normalized cross-correlation functions between the measured waveform and a sample of estimated waveforms for different positions on the surface is calculated. With the maximum coefficient of the normalized cross-correlation functions, the most likely position is determined. This estimated position can be refined by calculating additional normalized cross-correlation functions and the corresponding maximum coefficients in close neighborhood. This procedure is repeated until the highest maximum coefficient is found. Then the position on the known surface and the precise range value to the surface is determined.

Because of the radial symmetry of the sphere, which is investigated in Section 3.2, the position on the surface delivers a circle of possible positions around the center of the sphere surface. If the radius of the sphere is known, then at least one additional position on the surface has to be estimated to determine the correct sphere position.

The processing time for the position and range mainly depends on calculating the surface response. The surface response is determined by the spatial undersampling of the high resolution range and intensity image. The high-resolution range image with 300x300 pixels does not have any practical relevance if it is sufficiently large to not induce errors in a higher magnitude as those incurred by our discretized beam distribution. To decrease the processing time, a smaller high-resolution range image might be sufficient on the cost of less accuracy for the range estimation.

5. CONCLUSION

In this work we have presented a scheme to estimate the precise range and position of a known surface. We simulated the surface response for different slopes and a spherical surface. Estimated waveforms received from different positions on the sphere surface are shown. The data generation and analysis we carried out are general investigations for a laser system which records the full-waveform of laser pulses. The method remains to be tested with real data, and expanded to handle more complex geometries.

REFERENCES

Baltsavias EP (1999) Airborne laser scanning: existing systems and firms and other resources. ISPRS Journal of Photogrammetry & Remote Sensing 54: 164-198.

Blair JB, Rabine DL, Hofton MA (1999) The Laser Vegetation Imaging Sensor (LVIS): A medium-altitude, digitization-only, airborne laser altimeter for mapping vegetation and topography. ISPRS Journal of Photogrammetry & Remote Sensing 56: 112-122.

Brenner AC, Zwally HJ, Bentley CR, Csatho BM, Harding DJ, Hofton MA, Minster JB, Roberts LA, Saba JL, Thomas RH, Yi D (2003) Geoscience Laser Altimeter System (GLAS) - Derivation of Range and Range Distributions From Laser Pulse Waveform Analysis for Surface Elevations, Roughness, Slope, and Vegetation Heights. Algorithm Theoretical Basis Document - Version 4.1.

Bufton JL (1989) Laser Altimetry Measurements from Aircraft and Spacecraft. Proceedings of the IEEE, Vol. 77, No. 3, 463-477.

Der S, Redman B, Chellappa R (1997) Simulation of error in optical radar measurements. Applied Optics 36 (27), 6869-6874.

Dold C (2005) Extended Gaussian images for the registration of terrestrial scan data. In: Vosselman G, Brenner C (eds) Laserscanning 2005. International Archives of Photogrammetry and Remote Sensing. Vol. 36, Part 3/W19, 180-185.

Gardner CS (1982) Target signatures for laser altimeters: an analysis. Applied Optics, Volume 21, Issue 3, 448-453.

Hofton MA, Blair JB (2002) Laser altimeter return pulse correlation: A method for detecting surface topographic change. Journal of Geodynamics special issue on laser altimetry 34, 491-502.

Hofton MA, Minster JB, Blair JB (2000) Decomposition of laser altimeter waveforms. IEEE Transactions on Geoscience and Remote Sensing 38 (4), 1989–1996.

Hug C, Ullrich A, Grimm A (2004) LITEMAPPER-5600 - a waveform digitising lidar terrain and vegetation mapping system. International Archives of Photogrammetry, Remote Sensing and Spatial Information Sciences 36 (Part 8/W2), 24–29.

Huising EJ, Gomes Pereira LM (1998) Errors and accuracy estimates of laser data acquired by various laser scanning systems for topographic applications. ISPRS Journal of Photogrammetry & Remote Sensing 53: 245-261.

Irish JL, Lillycrop WJ (1999) Scanning laser mapping of the coastal zone: the SHOALS system. ISPRS Journal of Photogrammetry & Remote Sensing 54: 123-129.

Irish JL, McClung JK, and Lillycrop WJ (2000) Airborne lidar bathymetry: the SHOALS system. PIANC Bulletin. 2000 (103): 43-53.

Jelalian AW (1992) Laser Radar systems. Norwood, MA, Boston: Artech House.

Jutzi B, Eberle B, Stilla U (2002) Estimation and measurement of backscattered signals from pulsed laser radar. In: Serpico SB (ed) (2003) Image and Signal Processing for Remote Sensing VIII, SPIE Proc. Vol. 4885: 256-267.

Jutzi B, Stilla U (2003) Laser pulse analysis for reconstruction and classification of urban objects. In: Ebner H, Heipke C, Mayer H, Pakzad K (eds) Photogrammetric Image Analysis PIA'03. International Archives of Photogrammetry and Remote Sensing. Vol. 34, Part 3/W8, 151-156.

Jutzi B, Stilla U (2005) Measuring and processing the waveform of laser pulses. In: Gruen A, Kahmen H (eds) Optical 3-D Measurement Techniques VII. Vol. I, 194-203.

Kamermann GW (1993) Laser Radar. In: Fox CS (ed) Active Electro-Optical Systems, The Infrared & Electro-Optical Systems Handbook. Michigan: SPIE Optical Engineering Press.

Papoulis A (1984) Probability, Random Variables, and Stochastic Processes. Tokyo: McGraw-Hill.

Persson Å, Söderman U, Töpel J, Ahlberg S (2005) Visualization and analysis of full-waveform airborne laser scanner data. In: Vosselman G, Brenner C (Eds) Laser scanning 2005. International Archives of Photogrammetry and Remote Sensing 36 (3/W19), 109-114.

Reitberger J, Krzystek P, Heurich M (2006) Full-Waveform analysis of small footprint airborne laser scanning data in the Bavarian forest national park for tree species classification. In: Koukal T, Schneider W (Eds) 3D Remote Sensing in Forestry. 218-227.

Skolnik MI (1980) Introduction to radar systems. McGraw-Hill International Editions, Second Edition.

Söderman U, Persson Å, Töpel J, Ahlberg S (2005) On analysis and visualization of full-waveform airborne laser scanner data. Laser Radar Technology and Applications X. In: Kamerman W (ed) SPIE Proc. Vol. 5791: 184-192.

Steinvall O, Larsson H, Gustavsson F, Chevalier T, Persson Å, Klasén L (2004) Characterizing targets and backgrounds for 3D laser radars. Military Remote Sensing. In: Kamerman W, Willetts DV (eds) SPIE Proc. Vol. 5613: 51-66.

Steinvall O (2000) Effects of target shape and reflection on laser radar cross sections. Applied Optics 39 (24), 4381-4391.

Steinvall O, Carlsson T (2001) Three-dimensional laser radar modeling. In: Kamerman GW (Ed) Laser Radar Technology and Application VI, SPIE Proc. Vol. 4377, 23-34.

Thiel KH, Wehr A (2004) Performance Capabilities of Laser-Scanners - An Overview and Measurement Principle Analysis. International Archives of Photogrammetry, Remote Sensing and Spatial Information Sciences 36 (Part 8/W2), 14–18.

Thiel KH, Wehr A, Hug C (2005) A New Algorithm for Processing Fullwave Laser Scanner Data. EARSeL 3D-Remote Sensing Workshop, CDROM.

Vandapel N, Amidi O, Miller JR (2004) Toward Laser Pulse Waveform Analysis for Scene Interpretation. IEEE International Conference on Robotics and Automation (ICRA 2004).

Wagner W, Ullrich A, Briese C (2003) Der Laserstrahl und seine Interaktion mit der Erdoberfläche. Österreichische Zeitschrift für Vermessung & Geoinformation, VGI 4/2003, 223-235.

Wagner W, Ullrich A, Ducic V, Melzer T, Studnicka N (2006) Gaussian Decomposition and Calibration of a Novel Small-Footprint Full-Waveform Digitising Airborne Laser Scanner. ISPRS Journal of Photogrammetry & Remote Sensing, 60 (2), 100-112.

Wagner W, Ullrich A, Melzer T, Briese C, Kraus K (2004) From single-pulse to full-waveform airborne laser scanners: Potential and practical challenges. In: Altan MO (ed) International Archives of Photogrammetry and Remote Sensing. Vol 35, Part B3, 201-206.

Wehr A, Lohr U (1999) Airborne laser scanning – an introduction and overview. ISPRS Journal of Photogrammetry & Remote Sensing 54: 68-82.

Zwally HJ, Schutz B, Abdalati W, Abshire J, Bentley C, Brenner A, Bufton J, Dezio J, Hancock D, Harding D, Herring T, Minster B, Quinn K, Palm S, Spinhirne J, Thomas R (2002) ICESat's laser measurements of polar ice, atmosphere, ocean, and land. Journal of Geodynamics 34 (3–4), 405–445.